

Published in final edited form as:

Acc Chem Res. 2013 November 19; 46(11): . doi:10.1021/ar4000407.

Reversible, long-range radical transfer in *E. coli* class Ia ribonucleotide reductase

Ellen C. Minnihan[†], Daniel G. Nocera^{¶,*}, and JoAnne Stubbe^{†,‡,*}

[†]Department of Chemistry, Massachusetts Institute of Technology, 77 Massachusetts Avenue, Cambridge, MA 02139

[‡]Department of Biology, Massachusetts Institute of Technology, 77 Massachusetts Avenue, Cambridge, MA 02139

[¶]Department of Chemistry and Chemical Biology Harvard University, 12 Oxford Street, Cambridge, MA 02138

Introduction

Ribonucleotide reductases (RNRs) catalyze the conversion of nucleotides (NDPs or NTPs where N = C, U, G, or A) to 2'-deoxynucleotides (dNDPs or dNTPs)¹ and are responsible for controlling the relative ratios and absolute concentrations of cellular dNTP pools. For this reason, RNRs play a major role in ensuring the fidelity of DNA replication and repair. RNRs are found in all organisms and are classified based on the metal cofactor used to initiate catalysis,¹ with the class Ia RNRs requiring a diferric-tyrosyl radical (Y•) cofactor.

The prototypical class Ia RNR from *E. coli*, the subject of this account, is composed of two subunits, α and β , and is active as an $\alpha_2\beta_2$ complex, as highlighted in Figure 1. α houses the catalytic site for substrate (S) reduction and two allosteric effector (E = ATP, dGTP, TTP, and dATP) binding sites that govern which S is reduced (specificity site) and the overall rate of reduction (activity site). β contains the essential diferric-Y• cofactor. This unusually stable Y•, located at position 122, has a $t_{1/2}$ of 4 days at 4 °C in contrast to the μ s lifetimes observed for Y•s in solution. Nucleotide reduction occurs by a complex mechanism involving protein- and substrate-derived radicals, some details of which are summarized in Figure 2.^{1,3} The stable Y₁₂₂• transiently oxidizes a cysteine (C₄₃₉) in the catalytic site to a thiyl radical (S•), which reversibly abstracts a 3'-hydrogen atom (H•) from the NDP. The 3'-nucleotide radical rapidly loses water in the first irreversible step.^{1,3} The reducing equivalents are provided by two local cysteines (C₂₂₅ and C₄₆₂), and the resulting disulfide is re-reduced for subsequent turnovers, ultimately by thioredoxin (TR), thioredoxin reductase (TRR), and NADPH.

Uhlen and Eklund proposed a structure of the active $\alpha_2\beta_2$ complex by *in silico* docking of crystal structures of the individual subunits (Figure 1).² An atomic-resolution structure of an active class I RNR is still not available; however, recent experimental evidence supports this model (*vide infra*). The interaction between subunits is governed primarily by the flexible C-terminus of α (residues 360-375, Figure 1).⁴ The most provocative feature of the docking model was the >35 Å distance between Y₁₂₂• in α and C₄₃₉ in β . The long distance suggested that direct oxidation of C₄₃₉ by Y₁₂₂• by a singlestep, electron tunneling mechanism would be too slow (k_{ET} of 10^{-7} to 10^{-9} s⁻¹) to account for the turnover number

*To whom correspondence should be addressed: nocera@fas.harvard.edu, stubbe@mit.edu.

The authors declare no competing financial interests.

of the *E. coli* RNR ($\sim 10 \text{ s}^{-1}$).⁵ Accordingly, Uhlin and Eklund proposed that oxidation occurred by a hopping mechanism utilizing a specific pathway of conserved aromatic amino acids: Y₁₂₂• [W48?] Y₃₅₆ in β to Y₇₃₁ Y₇₃₀ C₄₃₉ in α . The necessity of these residues for catalysis was established by site-directed mutagenesis experiments.^{6,7}

The thermodynamics of Y or W oxidation require that proton transfer (PT) accompanies electron transfer (ET) at physiological pH. In RNR, these transfers are proposed to occur in a concerted fashion to prevent formation of high-energy, charged intermediates, thereby requiring a proton-coupled electron transfer (PCET) at each step.⁸⁻¹⁰ In our model, orthogonal PCET steps are operative in β , with the proton and electron transferring from the same donor to different acceptors, whereas co-linear PCET steps are operative in α , with the proton and electron moving between the same donor/acceptor pair (Figure 3a).^{7,10,11} Our current model for the thermodynamics of radical transfer (RT) has evolved from studies in which the reduction potentials have been modulated at each Y on the pathway (Figure 3b).¹²⁻¹⁴ It holds that the potentials increase from Y₁₂₂ < Y₃₅₆ < Y₇₃₁ \approx Y₇₃₀ C₄₃₉, with the uphill forward oxidation driven by irreversible loss of H₂O during nucleotide reduction. We now give an account of the results that have given rise to our RT mechanism and thermodynamic model.

Tools

Protein engineering

The study of RT is complicated by the fact that the PCET events are masked in the wild-type (wt) RNR by rate-limiting protein conformational changes that occur upon binding of nucleotides to β prior to RT.⁵ To perturb the native RT pathway in a predictable way, we have utilized two methods for site-specific incorporation of eight unnatural amino acids (UAAs) with altered reduction potentials and/or pK_as into RNR (Figure 4a, Table 1). One method involved the semisynthesis of β by expressed protein ligation (EPL),^{15,16} whereas the second utilized *in vivo* nonsense codon suppression.^{13,17} Current research utilizes the latter method, as it may be applied to any residue in either subunit, minimizes mutations to the native enzyme relative to EPL, and has allowed isolation of 100 mg quantities of protein (Figure 4b).

Kinetic techniques and spectroscopic methods

The reactivity of a mutant protein, once isolated, is studied by rapid kinetic techniques to unveil radical intermediates. In a typical experiment, a solution containing a mutant subunit (β or α) and S is rapidly mixed with a solution containing the complementary wt subunit and E, and the reaction monitored with millisecond time resolution for loss of Y₁₂₂• and formation of a new radical(s) (Figure 5). Changes can be monitored continuously by stopped-flow (SF) UV-vis or fluorescence spectroscopies, or discontinuously using either a rapid freeze quench (RFQ) apparatus and paramagnetic resonance spectroscopy or a rapid chemical quench (RCQ) apparatus and scintillation counting of a radiolabeled product.

Figure 6 shows the spectroscopic signatures of the stable diferric-Y₁₂₂• in β . The cofactor gives rise to a UV-vis spectrum with a sharp feature at 411 nm (Figure 6a) and an EPR spectrum (9 GHz) with hyperfine couplings associated with one of its two β -methylene protons and its 3,5 aromatic protons (Figure 6b). The *g* tensors [*g*_x, *g*_y, *g*_z] determined by high-field (HF) EPR (94 or 140 GHz) are particularly informative, as *g*_x is very sensitive to the electrostatic (i.e., H-bonding) environment of the Y• (Figure 6c). EPR and related methods, including pulsed electron-electron double resonance (PELDOR)²⁰ and HF [²H]-electron nuclear double resonance (ENDOR)²¹ spectroscopies, have allowed characterization of stable and transient radicals observed in engineered RNRs. Together, these methods have provided tools for the study of RT in RNR.

Complexities in studying *E. coli* class Ia RNR

Two unresolved issues have complicated our mechanistic studies. The first is the apparent half-sites reactivity of RNR,^{5,19} a phenomenon in which radical initiation occurs initially within a single / pair and a chemical or conformational step during or subsequent to product formation then triggers RT on the second / pair.⁵ The second RT event is prevented when a radical is trapped in the first / pair by replacing the S with a mechanism-based inhibitor²⁰ or by modulating the energetics of RT using UAAs.^{19,23} The second issue concerns the stoichiometry and distribution of Y_{122}^{\bullet} within 2. The diferric- Y^{\bullet} in 2 is self-assembled from apo- 2 to give $\sim 1.2 Y^{\bullet}/2$ and while the loading of radical in each monomer is unknown, our *in vitro* biochemical studies suggest it is evenly distributed ($0.6 Y^{\bullet}/$).

Evidence for a pathway of redox-active amino acids

Our earliest experiments sought to validate the proposed pathway and the redox reactivity of its constituents (Figure 3a). The role of Y_{356} in the C-terminal tail of 2 was first studied, as its position relative to other residues is unknown (Figure 1). Using EPL, Y_{356} was replaced with 3,4-dihydroxyphenylalanine (DOPA, 2, Figure 4a), which has a peak potential (E_p) 260 mV lower than Y (pH 7, Table 1) and was utilized as a radical trap. Reaction of Y_{356} DOPA- 2 with wt- 2, S, and E resulted in loss of 50% of the initial Y_{122}^{\bullet} concomitant with formation of an equal amount of $DOPA_{356}^{\bullet}$.¹⁹ No $DOPA_{356}^{\bullet}$ was observed in the absence of the second subunit or nucleotides. The kinetics of $DOPA_{356}^{\bullet}$ formation involved multiple phases, the majority of which were kinetically competent (i.e., faster than the wt k_{cat}); however, the mutant was unable to make dNDP. These studies demonstrated that nucleotides are required to trigger RT and provided the first evidence for conformation changes associated with RT.

Our attention turned to investigating the roles of Y_{731} and Y_{730} in 2. In collaboration with the Schultz lab, an orthogonal tRNA synthetase (RS) that specifically recognizes 3-aminotyrosine (NH_2Y , 3, Figure 4a) was evolved and was used to incorporate NH_2Y to positions 730 and 731 of 2 and 356 of 2 (collectively called NH_2Y -RNRs). With an E_p 190 mV lower than Y (pH 7, Table 1), NH_2Y was expected to behave like DOPA, as a radical sink. Indeed, reaction of each of the three NH_2Y -RNRs with the second subunit, S, and E resulted in the generation of an NH_2Y^{\bullet} kinetically coupled to Y_{122}^{\bullet} loss, as measured by SF UV-vis and EPR spectroscopy (Figure 7).^{17,24} Radical formation again required the presence of both subunits and nucleotides, was biphasic, and was kinetically competent for all S and E pairs for all three NH_2Y -RNRs. In contrast to DOPA, however, all NH_2Y -RNRs were active in dNDP production. Additional experiments revealed that NH_2Y^{\bullet} was formed only when the other Ys in the wt RT pathway were intact. This result was interpreted as evidence that NH_2Y^{\bullet} formation is pathway-dependent and not the indirect consequence of introducing a thermodynamic trap into the protein.²⁵ Thus, results obtained with DOPA- and NH_2Y -RNRs support the participation of three Ys acting as redox relays linking Y_{122}^{\bullet} in 2 to C_{439} in 2.

Evidence for an active $\alpha 2 \beta 2$ complex resembling the docking model

The ability to generate moderately stabilized NH_2Y^{\bullet} s ($t_{1/2}$ on min scale) at positions along the pathway coupled with the half-sites reactivity of RNR allowed us to test whether the docking model (Figure 1)² is an accurate representation of the active RNR. Specifically, PELDOR spectroscopy, a technique that detects weak dipolar interactions between paramagnetic species separated by 20-80 Å, was utilized to measure diagonal distances between a radical generated on the pathway in one / pair and the Y_{122}^{\bullet} on the second / pair (Figure 8). The distances measured between Y_{122}^{\bullet} and $DOPA_{356}^{\bullet}$ provided the first

structural constraint on the location of this residue within $\beta 2$. Measurements between Y_{122}^{\bullet} and $NH_2Y_{731}^{\bullet}$, $NH_2Y_{730}^{\bullet}$, or an active-site nitrogen-centered radical formed upon reaction with the mechanism-based inhibitor 2-azido-2-deoxyuridine 5-diphosphate (N_3UDP)¹ were all in excellent agreement with the distances predicted by the docking model.^{20,23}

We have also observed that generation of an NH_2Y^{\bullet} on the pathway induces a tight, kinetically stable $\beta 2/\beta 2$ interaction.²⁶ At low $\beta 2$ and $\beta 2$ concentrations in the presence of S and E pairs, the wt $\beta 2/\beta 2$ interaction is weak ($K_d = 50\text{-}400$ nM) and transient ($k_{off} \sim 50\text{-}100$ s⁻¹).^{4,27} In contrast, under conditions that generate $NH_2Y_{730}^{\bullet}$, the binding between $Y_{730}NH_2Y\text{-}\beta 2$ and wt- $\beta 2$ is tight ($K_d = 7$ nM), cooperative, and long-lived ($k_{off} \sim 10^{-3}$ s⁻¹). The stable complex has been structurally characterized by electron microscopy (30 Å resolution) and was found to be consistent with the docking model, providing the first direct visualization of RNR in a catalytically relevant state.²⁶

Mechanism of long-range PCET in *E. coli* RNR

pK_as of pathway residues

UAAs with perturbed pK_as (Figure 4a, **1** and **4-8**, and Table 1) provide a means to study the nature of the PT coupled to ET (i.e., orthogonal vs. co-linear PCET, Figure 3a). To interpret the results of such experiments, we initially determined the extent to which the pK_as of the pathway Ys are modulated by their local protein environment using NO_2Y (Figure 4, **1**). The absorbance features of the NO_2Y phenolate (NO_2Y^- , $\lambda_{max} = 430$ nm, $\epsilon = 4,200$ cm⁻¹ M⁻¹) allowed titration of a single residue in the 258 kDa complex of $\beta 2$, S and E. When incorporated at position 356 of $\beta 2$ and 730 and 731 of $\beta 2$, the pK_a of NO_2Y was increased by 1 pH unit compared that of NO_2Y in solution (7.2).^{15,28} In contrast, NO_2Y incorporated at position 122 of $\beta 2$ revealed an increase in pK_a by >2.5 units,²⁸ suggesting that the hydrophobic pocket surrounding the cofactor confers unique properties on Y_{122} relative to the other pathway Ys. X-ray structures of $\beta 2$ and $\beta 2$ mutants containing NO_2Y revealed minimal changes in comparison to structures of the respective wt subunits.^{28,29}

Mechanism of RT in $\beta 2$

Our proposal for orthogonal PCET in $\beta 2$ (Figure 3a) was first examined by replacing Y_{356} with 2,3-F₂Y (**5**, Figure 4a), which has a pK_a of 7.8.³⁰ A pH rate profile of dCDP formation with $Y_{356}(2,3)F_2Y\text{-}\beta 2$ and wt- $\beta 2$ revealed that the complex was active from pH 6-9, indicating that ET through position 356 does not require PT and suggesting that an H-bond to Y_{356} is not necessary for RT through that position.³⁰ Subsequently, a complete series of F_nYs (**4-8**, Figure 4a) with pK_as ranging from 5.6-7.8 (Table 1) were incorporated at position 356. In no case was a correlation between enzyme activity and protonation state observed, consistent with an orthogonal PCET mechanism.¹⁶

An orthogonal PCET mechanism involving 356 suggests the importance of a proton acceptor. This was proposed to be the conserved acid E_{350} in the C-terminus of $\beta 2$ (Figure 3a)⁶ after Sjöberg and colleagues observed that $E_{350}A\text{-}\beta 2$ is catalytically inactive despite maintaining its ability to bind $\beta 2$ and to assemble cofactor.⁶ Furthermore, reactions between $E_{350}A/Y_{356}NH_2Y\text{-}\beta 2$ and wt- $\beta 2$, or $E_{350}A\text{-}\beta 2$ and $Y_{731}NH_2Y\text{-}\beta 2$, fail to generate NH_2Y^{\bullet} , indicating that the E_{350} mutation prevents NH_2Y oxidation at positions 356 and 731.¹⁴ While these results highlight the importance of E_{350} in mediating RT through position 356, the inactivity of these and the $E_{350}D\text{-}$ and $E_{350}Q\text{-}\beta 2$ mutants prevents drawing strong mechanistic conclusions.

Mechanistic insight into the first step of RT, reduction of Y_{122}^{\bullet} , has been investigated in collaboration with the Bollinger/Krebs lab.³¹ The model (Figure 3a) proposes that Y_{122}^{\bullet}

reduction is coupled to PT from a Fe1-bound water. To test this hypothesis, the Mössbauer spectrum of the resting diferric-Y₁₂₂• in [⁵⁷Fe]-loaded wt- 2, wt- 2, and E was compared to that of the Y•-reduced cofactor generated upon reaction of 2, 2 and E with 2-N₃UDP.¹ The similarities in the isomer shifts and the differences in the quadrupole splitting parameter associated with Fe1 suggest no change in the Fe oxidation state and a change in ligation to Fe1 from a bound water to a bound hydroxide, consistent with PT from this ligand to the reduced Y₁₂₂.³¹

Mechanism of RT in α2

Experimental evidence for co-linear PCET within 2, suggested by the proximity of pathway residues in the 2 structure, was obtained by studying light-initiated RT in systems in which the 2 subunit is replaced by a photopeptide (Figure 9).^{7,10} The peptide corresponds to the C-terminal 19 amino acids (356-375) of (C19) with either a Y or F_nY at position 356 and a photooxidant (PO) such as benzophenone (BP), anthraquinone (Anq), or Re(bpy)(CO)₃CN ([Re]) appended to the N-terminus.^{10,11} Pairing different POs with different Y analogs allows modulation of the driving force of oxidation at position 356 and of radical injection into 2. Upon excitation, the PO generates a transient radical at 356, a small fraction of which migrates into 2 (Figure 9). The time-resolved formation and decay of the 356 radical is monitored by transient absorption spectroscopy.

Photolysis of either [BP]- or [Anq]-Y-C19 with wt- 2, [¹⁴C]-CDP, and ATP under single-turnover conditions generated 0.25 dCDP/ 2, demonstrating the chemical competence of the system.³² The redox-inert Y₇₃₀F- 2 prevented dCDP formation, supporting co-linear transport of an H⁺ and e⁻.³² The light-initiated reaction of [Re]-2,3,6-F₃Y-C19 with wt- 2 was compared to that with various 2 mutants to investigate whether the photogenerated F₃Y₃₅₆• could initiate RT into 2. Radical injection occurred with a *k*_{et} of ~10⁵ s⁻¹ in both the wt enzyme and C₄₃₉S mutant, but was not observed in the Y₇₃₁F and Y₇₃₀F variants. These results suggest that the intact Y₇₃₁/Y₇₃₀ dyad and its associated H-bonding network are necessary for RT.³³ Experiments are underway to test this hypothesis with [Re]-C₃₅₅S-2, a mutant 2 in which the PO is attached at position 355, in the intact 2 2 complex.³⁴

Additional support for co-linear PCET within 2 has been obtained from studies of the NH₂Y₇₃₀• formed upon reaction of Y₇₃₀NH₂Y- 2 with wt- 2, CDP, and ATP by HF-EPR and ENDOR spectroscopies. Multifrequency EPR analysis of [¹⁴N]- and [¹⁵N]-NH₂Y₇₃₀• in H₂O and D₂O allowed for accurate simulations of experimental spectra and revealed an unusually low *g*_x value of 2.0052, suggesting the importance of a local H-bonding environment.³⁵ Analysis of ND₂Y₇₃₀• using HF [²H]-ENDOR spectroscopy (Figure 10), combined with structural information²⁴ and DFT calculations, allowed assignment of exchangeable protons in the immediate vicinity of the NH₂Y₇₃₀•.²¹ These studies revealed strong intramolecular H bonds from the NH₂ group, two moderate H-bonding interactions (presumably with the adjacent pathway residues, Y₇₃₁ and C₄₃₉), and a weaker interaction likely associated with an ordered water molecule. These results support a co-linear PCET mechanism within 2 by demonstrating a structured H-bonding network in the active 2 2 complex.²¹

Mapping the thermodynamic landscape of the PCET pathway

A barrier to the RT pathway: NO₂Y or F_nY

UAAs incorporated into RNR alter the thermodynamics from 260 mV easier to oxidize (DOPA) to 190 mV harder to oxidize (NO₂Y) than Y based on E_p measurements near physiological pH (Table 1). When the Y at position 356, 731, or 730 is replaced with NO₂Y, the resulting mutant is inactive indicating that NO₂Y cannot be oxidized by other pathway

radicals and hence cannot support RT. A series of F_nY s (4-8, Figure 4a, Table 1) incorporated at position 356 of Δ by EPL provided access to E_p s that varied from -50 mV to $+250$ mV relative to Y in the pH 6-9 range in which RNR is active (Figure 11).¹⁸ pH rate profiles of these mutants demonstrated that their activities fell into three regimes based on the difference in E_p (E_{ps}) between the F_nY (or F_nY^-)/ F_nY^\bullet and Y/Y^\bullet couples. $Y_{356}F_nY$ - Δ s had activities resembling wt- Δ at $E_{ps} < 80$ mV, whereas they were inactive at $E_{ps} < 200$ mV, consistent with the results of NO_2Y mutants. In the range from 80-200 mV, $Y_{356}F_nY$ - Δ s exhibited measurable activities that decreased with increasing E_p .¹⁶

A sink in the RT pathway: DOPA or NH_2Y

Substitution of pathway residues by DOPA or NH_2Y (2 and 3, Figure 4a) has allowed us to explore the consequence of lowering the potential at positions on the pathway by 260 and 190 mV, respectively (Table 1). As noted above, $Y_{356}DOPA$ - Δ is catalytically inactive, presumably due to the inability of $DOPA_{356}^\bullet$ to oxidize Y_{731} . We expected that NH_2Y -RNRs would also be inactive, however these three mutants possessed 3-12% of the activity of their corresponding wt subunits.^{17,24} (Footnote 1: This result was unexpected, as the E_p between Y and NH_2Y is near the 200 mV threshold observed to shut down RT. However, the E_{ps} reported herein (Table 1)^{15,17-19} have been measured by various methods by different researchers, and thus significant error could exist in our calculated E_{ps} . We are collaborating with the Koppenol lab to re-measure the potentials of these UAAs to obtain a single set of reliable values. Further error arises from the fact that E_p values are sensitive to the reaction conditions under which they were measured, and thus the observed E_{ps} may differ significantly from true reduction potentials (E° s).) The combination of kinetically competent NH_2Y^\bullet formation and catalytic dNDP formation in NH_2Y -RNRs present an opportunity to measure solvent isotope effects at individual steps in the RT pathway and during NDP reduction, providing insight on mechanistic details that are kinetically masked in the wt enzyme.¹⁴ In summary, activity measurements of RNRs containing UAAs indicate that the thermodynamics of RT can be modulated by ± 200 mV relative to the native pathway at positions 356, 731, and 730 while retaining some enzymatic activity.

Increasing the driving force of RT at position 122: NO_2Y and F_nY s

In an effort to characterize the native Y^\bullet intermediates, we replaced Y_{122} with NO_2Y and F_nY s (1 and 4-7, Figure 4a). We anticipated the ability to generate radicals of NO_2Y and F_nY s at this position given the unique mechanism of diferric- Y_{122}^\bullet assembly in the wt enzyme, which utilizes a strongly oxidizing Fe^{3+}/Fe^{4+} intermediate ("X," Figure 12).⁷ A three-syringe, double-mixing apparatus was employed for these experiments in which Fe^{II} -loaded $Y_{122}NO_2Y$ - Δ was rapidly mixed with O_2 -saturated buffer to generate $NO_2Y_{122}^\bullet$ (1.2 eq/ Δ , $t_{1/2} \sim 40$ s at 25 °C) on the first syringe drive, followed immediately by reaction of this short-lived $NO_2Y_{122}^\bullet$ with wt- Δ , S, and E on the second syringe drive (Scheme 1, step 1).²⁹ The reaction was monitored by SF, RFQ-EPR, RFQ-PELDOR and RCQ methods (Figure 5) and the results are summarized in Scheme 1.²⁹ After assembly of the active cofactor, $NO_2Y_{122}^\bullet$ is rapidly reduced (>100 s⁻¹) in the first step of RT to generate the phenolate ($NO_2Y_{122}^-$) rather than the anticipated phenol, indicating an uncoupling of PT from ET. All subsequent steps, including formation of dCDP and a new Y^\bullet (s), occurred with similar rate constants (>100 s⁻¹). The ability to detect dCDP and new Y^\bullet formation at rate constants 10- to 50-fold faster than the wt k_{cat} indicated that disruption of the PT/ET coupling in the first step bypassed the conformational change that is rate-determining in the wt enzyme. Only 0.6 eq dCDP/ Δ and 0.6 eq Y^\bullet / Δ were generated in this process, indicating that the mutant enzyme (1.2 $NO_2Y_{122}^\bullet$ / Δ) could perform only a single turnover with half-sites reactivity, presumably due to inability to reoxidize the $NO_2Y_{122}^-$ to $NO_2Y_{122}^\bullet$ during reverse RT.

The results of additional studies of NO₂Y-containing 2s with either additional mutations of pathway residues (Y-to-F or Y-to-3,5-F₂Y) or globally labeled -[2H]-Ys, in conjunction with HF EPR and PELDOR spectroscopies, indicated that the observed Y• is generated during reverse RT and exists as an equilibrium of radicals at positions 356, 731, and 730 in ~10:1:1 ratio.^{12,29} These findings provide the basis for the relative positioning of Y₃₅₆, Y₇₃₁, and Y₇₃₀ in the proposed thermodynamic landscape of the RT pathway (Figure 3b).¹²

To explore reactivity in the ~200 mV regime separating NO₂Y and Y, a series of F_nYs (4-7, Figure 4a) were incorporated in place of Y₁₂₂. Assuming that Y₁₂₂F_nY- 2s experience a pK_a perturbation similar to that of NO₂Y₁₂₂ (>2.5 units),²⁸ all F_nYs would remain protonated at pH 7.6 and would vary from 50 mV easier to 100 mV harder to oxidize than Y (Figures 3b and 11).¹⁸ Using an evolved, polyspecific F_nY-RS, four Y₁₂₂F_nY- 2s were isolated, and the assembly and stability of their F_nY₁₂₂•s were spectroscopically characterized.^{13,14} Their EPR spectra feature hyperfine couplings of the radical to the fluorine nuclei, giving rise to sharp low- and high-field features that facilitate spectral deconvolution of F_nY₁₂₂•s from pathway Y•s (Figure 13a).¹³ All Y₁₂₂F_nY- 2s are active in the steady-state with 10-100 % the activity of wt- 2.14 When the driving force of RT is raised relative to Y, reaction of Y₁₂₂F_nY- 2s with wt- 2 (or Y₇₃₁F- 2), S, and E resulted in loss of F_nY₁₂₂• concomitant with the generation of a new radical, hypothesized to be Y₃₅₆• generated during forward RT (Figure 13b).^{13,14} The kinetics of new radical formation and dCDP production have been studied for the reaction of Y₁₂₂(2,3,5)F₃Y- 2 with wt- 2, CDP, and ATP, and indicate that Y₃₅₆• formation is kinetically competent relative to dCDP formation.¹⁴

Finally, the ability to monitor oxidation of Y₃₅₆ by NO₂Y₁₂₂• or F_nY₁₂₂•s has allowed us to address the function of W₄₈ (Figure 3a).^{2,7} This residue has been shown to participate during *in vitro* cofactor assembly, but its role in long-range RT has not been established. Preliminary studies of the reactivity of Y₁₂₂NO₂Y/Y₃₅₆F- 2 or Y₁₂₂(2,3,5)F₃Y/Y₃₅₆F- 2 double mutants provided no evidence for the formation of a discrete W₄₈•/W₄₈•+ intermediate during in RT, although it is possible that W₄₈ plays an important role in conformational gating.^{13,14,29}

From the studies conducted to date, a thermodynamic landscape for the RT pathway is emerging (Figure 3b). This model indicates that position 122 is the pathway minimum, however, detection of Y₃₅₆• in the reaction with Y₁₂₂(2,3,5)F₃Y- 2 as a radical initiator suggests that the thermodynamic difference between position 122 and 356 is small and that the stability of Y₁₂₂• may be kinetic in origin. W₄₈ is colored in gray, as we currently have no evidence in support of its participation as a discrete radical intermediate. The three transiently oxidized Ys are harder to oxidize than Y₁₂₂, with Y₇₃₁ and Y₇₃₀ 50-100 mV harder to oxidize than Y₃₅₆ and roughly isoenergetic with one another.¹² Finally, C₄₃₉ is placed at a reduction potential quite similar to or slightly elevated above the 730/731 dyad based on the solution reduction potential of glutathione radical at neutral pH.³⁶ In our model, the forward RT pathway is thus uphill, and C₄₃₉ oxidation is driven by the rapid, irreversible loss of water in the second step of nucleotide reduction (Figure 2),^{1,3} and the reverse RT pathway is downhill and rapid.

Conclusions

This account summarizes the results of recent mechanistic studies on mutant *E. coli* class Ia RNRs containing unnatural Y analogs at the proposed sites of stable and transient Y• formation on the RT pathway. Specifically, the results obtained from unnatural DOPA-, NH₂Y-, NO₂Y- and F_nYs-RNRs and light-initiated photo-RNRs, were used to establish: (1) that there exists a specific pathway containing a minimum of four Ys involved in long-range RT over 35 Å across a compact, globular 2 × 2 resembling Uhlin and Eklund's docking

model; (2) that RT occurs by orthogonal and co-linear PCET transfers in the α and β subunits, respectively; (3) that the overall thermodynamics of RT are only slightly uphill in the forward direction, with several of the intervening steps being nearly isoenergetic; (4) that the individual RT steps and the chemistry of nucleotide reduction are fast ($\sim 10^5 \text{ s}^{-1}$ and $>100 \text{ s}^{-1}$, respectively), despite being kinetically masked by several conformational changes ($10\text{-}100 \text{ s}^{-1}$) that occur when nucleotides bind to α and β ; and (5) that the rate-limiting conformational changes likely target the RT pathway and its tightly coupled proton and electron transfers.

Acknowledgments

We would like to thank the many researchers with whom we have fruitfully collaborated on this project, and we regret that space constraints have prevented us from recognizing each of them and their unique contributions in this account. We thank Arturo Pizano for assistance with Figure 9. This work was supported by the NIH grants GM47274 (to DGN) and GM29595 (to JS).

Biography

Ellen C. Minnihan conducted graduate research in the Stubbe lab and earned her PhD in Chemistry from MIT in 2012.

Daniel G. Nocera is the Patterson Rockwood Professor of Energy at Harvard University. His research focuses on the study of PCET as it pertains to the biology of nucleotide metabolism and energy conversion.

JoAnne Stubbe, the Novartis Professor of Chemistry and Professor of Biology at MIT, has dedicated her career to the study of the mechanisms of ribonucleotide reductases and other enzymatic systems.

ABBREVIATIONS

α	RNR large subunit
β	RNR small subunit
E	effector
E_p	peak potential
ET	electron transfer
HF	high-field
$N_3\text{UDP}$	2-azido-2-deoxyuridine 5-diphosphate
PCET	proton-coupled electron transfer
PO	photooxidant
PT	proton transfer
RT	radical transfer
$S\cdot$	cysteine radical
S	substrate
UAA	unnatural amino acid
wt	wild-type
$Y\cdot$	tyrosyl radical

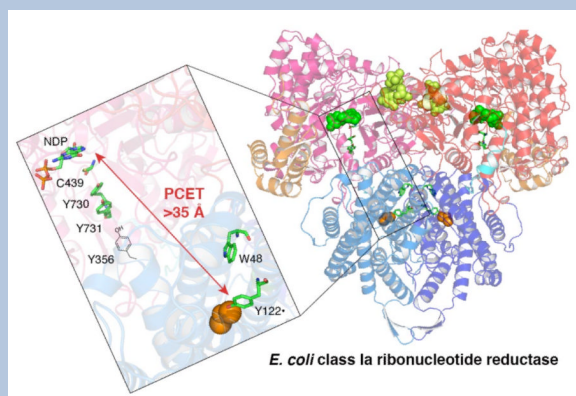
References

- (1). Stubbe J, van der Donk WA. Protein radicals in enzyme catalysis. *Chem. Rev.* 1998; 98:705–762. and references therein. [PubMed: 11848913]
- (2). Uhlin U, Eklund H. Structure of ribonucleotide reductase protein R1. *Nature.* 1994; 370:533–539. [PubMed: 8052308]
- (3). Licht S, Stubbe J. Mechanistic investigations of ribonucleotide reductases. *Compr. Nat. Prod. Chem.* 1999; 5:163–203. and references therein.
- (4). Climent I, Sjöberg BM, Huang CY. Carboxyl-terminal peptides as probes for *Escherichia coli* ribonucleotide reductase subunit interaction: kinetic analysis of inhibition studies. *Biochemistry.* 1991; 30:5164–5171. [PubMed: 2036382]
- (5). Ge J, Yu G, Ator MA, Stubbe J. Pre-steady-state and steady-state kinetic analysis of *E. coli* class I ribonucleotide reductase. *Biochemistry.* 2003; 42:10071–10083. [PubMed: 12939135]
- (6). Climent I, Sjöberg BM, Huang CY. Site-directed mutagenesis and deletion of the carboxyl terminus of *Escherichia coli* ribonucleotide reductase protein R2 - effects on catalytic activity and subunit interaction. *Biochemistry.* 1992; 31:4801–4807. [PubMed: 1591241]
- (7). Stubbe J, Nocera DG, Yee CS, Chang MCY. Radical initiation in the class I ribonucleotide reductase: long-range proton-coupled electron transfer? *Chem. Rev.* 2003; 103:2167–2201. and references therein. [PubMed: 12797828]
- (8). Cukier RI, Nocera DG. Proton-coupled electron transfer. *Annu. Rev. Phys. Chem.* 1998; 49:337–369. [PubMed: 9933908]
- (9). Mayer JM. Proton-coupled electron transfer: a reaction chemist's view. *Annu. Rev. Phys. Chem.* 2004; 55:363–390. [PubMed: 15117257]
- (10). Reece SY, Hodgkiss JM, Stubbe J, Nocera DG. Proton-coupled electron transfer: the mechanistic underpinning for radical transport and catalysis in biology. *Phil. Trans. Royal Soc. Lond. B Biol. Sci.* 2006; 361:1351–1364. and references therein.
- (11). Reece SY, Nocera DG. Proton-coupled electron transfer in biology: results from synergistic studies in natural and model systems. *Annu. Rev. Biochem.* 2009; 78:673–699. and references therein. [PubMed: 19344235]
- (12). Yokoyama K, Smith AA, Corzilius B, Griffin RG, Stubbe J. Equilibration of tyrosyl radicals (Y356•, Y731•, Y730•) in the radical propagation pathway of the *Escherichia coli* class Ia ribonucleotide reductase. *J. Am. Chem. Soc.* 2011; 133:18420–18432. [PubMed: 21967342]
- (13). Minnihan EC, Young DD, Schultz PG, Stubbe J. Incorporation of fluorotyrosines into ribonucleotide reductase using an evolved, polyspecific aminoacyl-tRNA synthetase. *J. Am. Chem. Soc.* 2011; 133:15942–15945. [PubMed: 21913683]
- (14). Minnihan, EC. Ph.D. Thesis. Massachusetts Institute of Technology; 2012.
- (15). Yee CS, Seyedsayamdost MR, Chang MCY, Nocera DG, Stubbe J. Generation of the R2 subunit of ribonucleotide reductase by intein chemistry: insertion of 3-nitrotyrosine at residue 356 as a probe of the radical initiation process. *Biochemistry.* 2003; 42:14541–14552. [PubMed: 14661967]
- (16). Seyedsayamdost MR, Yee CS, Reece SY, Nocera DG, Stubbe J. pH rate profiles of F_nY₃₅₆-R2s (n = 2, 3, 4) in *Escherichia coli* ribonucleotide reductase: evidence that Y₃₅₆ is a redox-active amino acid along the radical propagation pathway. *J. Am. Chem. Soc.* 2006; 128:1562–1568. [PubMed: 16448127]
- (17). Seyedsayamdost MR, Xie J, Chan CT, Schultz PG, Stubbe J. Site-specific insertion of 3-aminotyrosine into subunit 2 of *E. coli* ribonucleotide reductase: direct evidence for involvement of Y730 and Y731 in radical propagation. *J. Am. Chem. Soc.* 2007; 129:15060–15071. [PubMed: 17990884]
- (18). Seyedsayamdost MR, Reece SY, Nocera DG, Stubbe J. Mono-, di-, tri-, and tetra-substituted fluorotyrosines: new probes for enzymes that use tyrosyl radicals in catalysis. *J. Am. Chem. Soc.* 2006; 128:1569–1579. [PubMed: 16448128]
- (19). Seyedsayamdost MR, Stubbe J. Site-specific replacement of Y₃₅₆ with 3,4-dihydroxyphenylalanine in the 2 subunit of *E. coli* ribonucleotide reductase. *J. Am. Chem. Soc.* 2006; 128:2522–2523. [PubMed: 16492021]

- (20). Bennati M, Robblee JH, Mugnaini V, Stubbe J, Freed JH, Borbat P. EPR distance measurements support a model for long-range radical initiation in *E. coli* ribonucleotide reductase. *J. Am. Chem. Soc.* 2005; 127:15014–15015. [PubMed: 16248626]
- (21). Argirevic T, Riplinger C, Stubbe J, Neese F, Bennati M. ENDOR spectroscopy and DFT calculations: Evidence for the hydrogen-bond network within a2 in the PCET of *E. coli* ribonucleotide reductase. *J. Am. Chem. Soc.* 2012; 134:17661–17670. [PubMed: 23072506]
- (22). Gerfen GJ, Bellew BF, Un S, Joseph M, Bollinger J, Stubbe J, Griffin RG, Singel DJ. High-frequency (139.5 GHz) EPR spectroscopy of the tyrosyl radical in *Escherichia coli* ribonucleotide reductase. *J. Am. Chem. Soc.* 1993; 115:6420–6421.
- (23). Seyedsayamdost MR, Chan CT, Mugnaini V, Stubbe J, Bennati M. PELDOR spectroscopy with DOPA-2 and NH₂Y-2s: distance measurements between residues involved in the radical propagation pathway of *E. coli* ribonucleotide reductase. *J. Am. Chem. Soc.* 2007; 129:15748–15749. [PubMed: 18047343]
- (24). Minnihan EC, Seyedsayamdost MR, Uhlin U, Stubbe J. Kinetics of radical intermediate formation and deoxynucleotide production in 3-aminotyrosine-substituted *Escherichia coli* ribonucleotide reductases. *J. Am. Chem. Soc.* 2011; 133:9430–9440. [PubMed: 21612216]
- (25). Minnihan EC, Seyedsayamdost MR, Stubbe J. Use of 3-aminotyrosine to examine the pathway dependence of radical propagation in *Escherichia coli* ribonucleotide reductase. *Biochemistry.* 2009; 48:12125–12132. [PubMed: 19916558]
- (26). Minnihan EC, Ando N, Brignole EJ, Olshansky L, Chittuluru J, Asturias F, Drennan CL, Nocera DG, Stubbe J. Generation of a stable, aminotyrosyl radical-induced 2-2 complex of *E. coli* class Ia RNR. *Proc. Natl. Acad. Sci. US A.* 2013; 110:3835–3840.
- (27). Hassan, AQ.; Olshansky, L.; Yokoyama, K.; Nocera, DG.; Stubbe, J. In revision
- (28). Yokoyama K, Uhlin U, Stubbe J. Site-specific incorporation of 3-nitrotyrosine as a probe of pKa perturbation of redox-active tyrosines in ribonucleotide reductase. *J. Am. Chem. Soc.* 2010; 132:8385–8397. [PubMed: 20518462]
- (29). Yokoyama K, Uhlin U, Stubbe J. A hot oxidant, 3-NO₂Y122 radical, unmasks conformational gating in ribonucleotide reductase. *J. Am. Chem. Soc.* 2010; 132:15368–15379. [PubMed: 20929229]
- (30). Yee CS, Chang MCY, Ge J, Nocera DG, Stubbe J. 2,3-difluorotyrosine at position 356 of ribonucleotide reductase R2: A probe of long-range proton-coupled electron transfer. *J. Am. Chem. Soc.* 2003; 125:10506–10507. [PubMed: 12940718]
- (31). Wörsdörfer, B.; Conner, DA.; Yokoyama, K.; Seyedsayamdost, M.; Jiang, W.; Stubbe, J.; Martin, J.; Bollinger, J.; Krebs, C. Function of the diiron cluster in *Escherichia coli* class Ia ribonucleotide reductase in proton-coupled electron transfer. In revision
- (32). Reece SY, Seyedsayamdost MR, Stubbe J, Nocera DG. Photoactive peptides for light-initiated tyrosyl radical generation and transport into ribonucleotide reductase. *J. Am. Chem. Soc.* 2007; 129:8500–8509. [PubMed: 17567129]
- (33). Holder PG, Pizano AA, Anderson BL, Stubbe J, Nocera DG. Deciphering radical transport in the large subunit of class I ribonucleotide reductase. *J. Am. Chem. Soc.* 2012; 134:1172–1180. [PubMed: 22121977]
- (34). Pizano AA, Lutterman DA, Holder PG, Teets TS, Stubbe J, Nocera DG. Photo-ribonucleotide reductase 2 by selective cysteine labeling with a radical phototrigger. *Proc. Natl. Acad. Sci. US A.* 2011; 109:39–43.
- (35). Seyedsayamdost MR, Argirevic T, Minnihan EC, Stubbe J, Bennati M. Structural examination of the transient 3-aminotyrosyl radical on the PCET pathway of *E. coli* ribonucleotide reductase by multifrequency EPR spectroscopy. *J. Am. Chem. Soc.* 2009; 131:15729–15738. [PubMed: 19821570]
- (36). Madej E, Wardman P. The oxidizing power of the glutathione thiol radical as measured by its electrode potential at physiological pH. *Arch. Biochem. Biophys.* 2007; 462:94–102. [PubMed: 17466930]

CONSPECTUS

Ribonucleotide reductases (RNRs) catalyze the conversion of nucleotides to 2-deoxynucleotides and are classified on the basis of the metallo-cofactor used to conduct this chemistry. The class Ia RNRs initiate nucleotide reduction when a stable diferric-tyrosyl radical (Y^{\bullet} , $t_{1/2}$ of 4 days at 4 °C) cofactor in the α_2 subunit transiently oxidizes a cysteine to a thiyl radical (S^{\bullet}) in the active site of the β_2 subunit. In the active $\alpha_2\beta_2$ complex of the class Ia RNR from *E. coli*, this oxidation has been proposed to occur reversibly over 35 Å by a radical hopping mechanism along a specific pathway comprising redox-active aromatic amino acids: Y_{122}^{\bullet} [W₄₈?] Y_{356} in α_2 to Y_{731} Y_{730} C_{439} in β_2 , with each step necessitating a proton-coupled electron transfer (PCET). Protein conformational changes constitute the rate-limiting step in the overall catalytic scheme, thereby kinetically masking the detailed chemistry of the PCET steps. Technology has evolved to allow the site-selective replacement of the four pathway Ys with unnatural Y analogs. Rapid kinetic techniques combined with multi-frequency electron paramagnetic resonance, pulsed electron-electron double resonance, and electron nuclear double resonance spectroscopies have facilitated analysis of stable and transient radical intermediates in these mutants, thereby beginning to reveal the mechanistic underpinnings of the radical transfer (RT) process.



This account summarizes recent mechanistic studies on mutant *E. coli* RNRs containing the following Y analogs: 3,4-dihydroxyphenylalanine (DOPA) or 3-aminotyrosine (NH_2Y), both thermodynamic radical traps; 3-nitrotyrosine (NO_2Y), a thermodynamic barrier and probe of local environmental perturbations to the phenolic pK_a ; and fluorotyrosines (F_nYs , $n = 2$ or 3), dual reporters on local pK_a s and reduction potentials. These studies have established the existence of a specific pathway spanning 35 Å within a globular $\alpha_2\beta_2$ complex that involves one stable (position 122) and three transient (positions 356, 730, and 731) Y^{\bullet} s. Our results also support that RT occurs by an orthogonal PCET mechanism within α_2 , with Y_{122}^{\bullet} reduction accompanied by proton transfer from an Fe1-bound water in the diferric cluster and Y_{356} oxidation coupled to an off-pathway proton transfer likely involving E_{350} . In β_2 , RT likely occurs by a co-linear PCET mechanism, as evidenced from studies of light-initiated radical propagation from photopeptides mimicking the β_2 subunit to the intact β_2 subunit, and by [2H]-ENDOR spectroscopic analysis of the hydrogen-bonding environment surrounding a stabilized NH_2Y^{\bullet} formed at position 730. Additionally, studies on the thermodynamics of the RT pathway reveal that the relative reduction potentials decrease according to $Y_{122} < Y_{356} < Y_{731} \approx Y_{730} < C_{439}$, and that the pathway in the forward direction is thermodynamically unfavorable, with C_{439} oxidation likely driven by rapid, irreversible loss of water during the nucleotide reduction process. Kinetic studies of radical intermediates reveal that RT is gated by conformational changes occurring on the order of $> 100 \text{ s}^{-1}$ in addition to the

changes that are rate-limiting in the wt enzyme ($\sim 10 \text{ s}^{-1}$). The rate constant of one of the PCET steps is $\sim 10^5 \text{ s}^{-1}$, as measured in photo-initiated experiments.

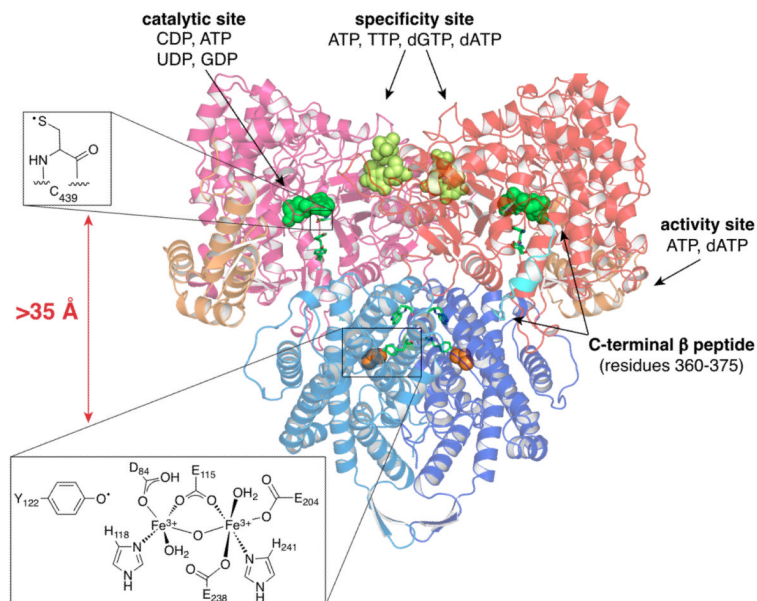


Figure 1.

A docking model of the *E. coli* β β' complex.² β (pink and red) contains three nucleotide binding sites. β' (light and dark blue) contains the diferric- Y^\bullet cofactor; residues 340 to 375 are not resolved in this structure. A peptide corresponding to the C-terminal 20 amino acids of β' is bound to each β , a portion of which (residues 360-375) is resolved in the crystal structure (cyan). The “ATP cone” region of β , which contains the effector site that governs activity, is colored orange. This model separates Y_{122}^\bullet in β from C_{439} in β by $>35 \text{ \AA}$. GDP (green), TTP (yellow) and the Fe_2O core of the diferric cluster (orange) are shown in CPK space-filling models. Residues constituting the RT pathway (green) are shown in sticks.

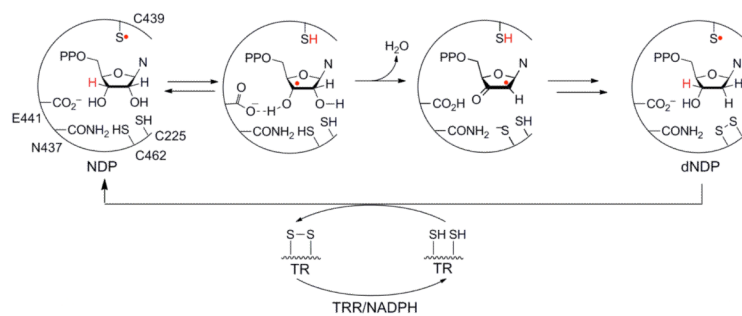
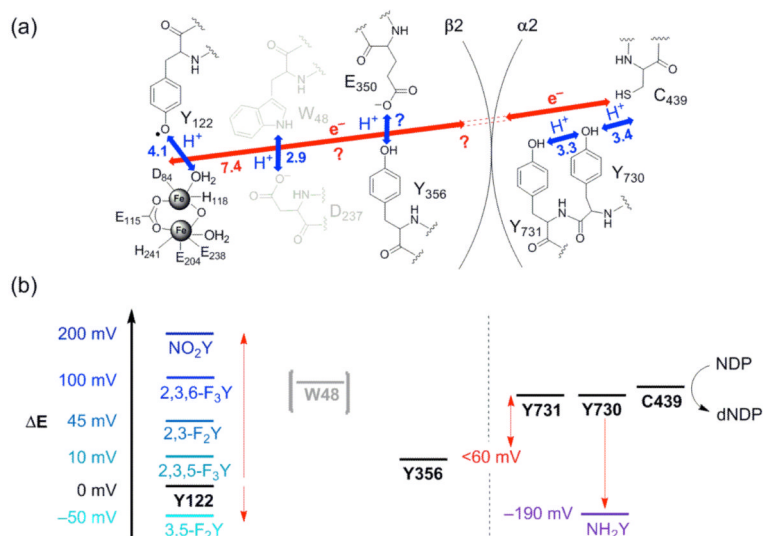


Figure 2. Mechanism of NDP reduction by RNR. The S• shown on C₄₃₉ of **2** in the first reaction step is reversibly generated by Y₁₂₂• in **2** by the mechanism shown in Figure 3a.

**Figure 3.**

The Nocera/Stubbe elaboration of the Uhlin/Eklund model for RT in *E. coli* class Ia RNR.

(a) The proposed movement of protons (blue arrows) and electrons (red arrows) at each step on the pathway. Distances (Å) are from structures of 2 and 2. E₃₅₀ and Y₃₅₆ are disordered in all 2 structures, and their positions are unknown. There is no direct evidence that W₄₈ and D₂₃₇ participate in RT and thus they are shown in gray. The distance between W₄₈ and Y₇₃₁ is modeled to be 25 Å. (b) The proposed relative reduction potentials of residues on the RT pathway from experiments using the indicated UAAs site-specifically incorporated in place of each Y. NH₂Y has been incorporated at position 356, 730, or 731. Note that the absolute reduction potentials of these residues, the structures of which are shown in Figure 4, are not known, and the relative reduction potentials indicated are our best estimates given current knowledge (see Table 1 and Footnote 1).

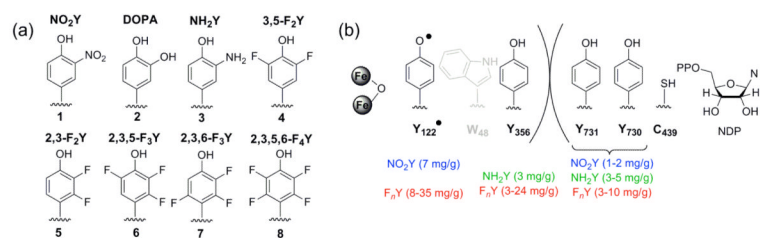


Figure 4.

UAAs incorporated into *E. coli* class Ia RNR. (a) Compounds **1-2** and **4-8** have been incorporated in position 356 of **2** by EPL, while compounds **1, 3-7** have been incorporated to sites in both **2** and **2** by *in vivo* nonsense suppression. (b) Purified protein yields achieved by *in vivo* nonsense suppression are given in parenthesis for each UAA at each position (in mg protein/g cells).

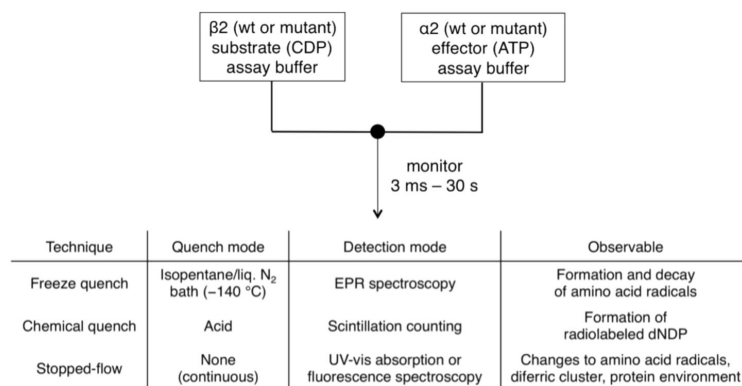


Figure 5. Experimental design, kinetic techniques, and detection methods for studying RT.

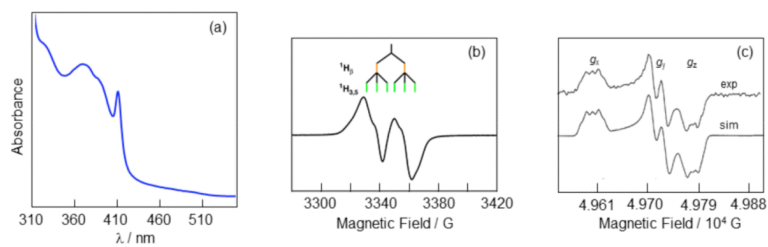


Figure 6. Spectroscopic characterization of the diferric- Y_{122}^\bullet cofactor from *E. coli* class Ia RNR. (a) The UV-vis spectrum has contributions from the diferric cluster at 325 and 365 nm and Y_{122}^\bullet at 411 nm. (b) The 9 GHz EPR spectrum of Y_{122}^\bullet with the origin of its hyperfine couplings indicated. (c) The 140 GHz EPR spectrum of Y_{122}^\bullet resolves three distinct g tensors. Adapted from reference 22.

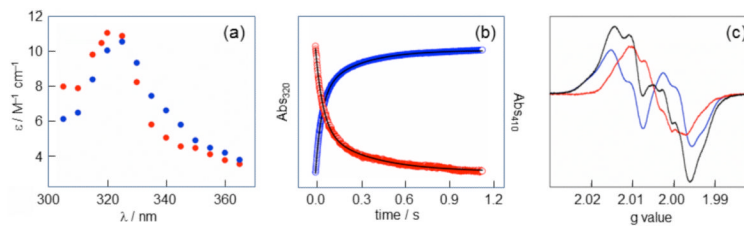


Figure 7.

Spectroscopic characterization of $\text{NH}_2\text{Y}\bullet\text{s}$. (a) A point-by-point reconstruction of the absorbance spectra of $\text{NH}_2\text{Y}_{730}\bullet$ (blue) and $\text{NH}_2\text{Y}_{731}\bullet$ (red) formed 1.5 s after reacting $\text{Y}_{731}\text{NH}_2\text{Y}-2$ (or $\text{Y}_{730}\text{NH}_2\text{Y}-2$) with wt-2, CDP, and ATP. (b) Averaged single-wavelength SF UV-vis traces for the $\text{Y}_{731}\text{NH}_2\text{Y}-2$ reaction described in (A). Loss of $\text{Y}_{122}\bullet$ (red, 410 nm) correlates with the formation of $\text{NH}_2\text{Y}_{731}\bullet$ (blue, 320 nm). Biexponential fits to the data are shown as black lines. (c) The 9 GHz EPR spectrum (black) of an identical reaction frozen after 10 s is a ~1:1 composite of residual $\text{Y}_{122}\bullet$ (blue) and $\text{NH}_2\text{Y}_{731}\bullet$ (red). Figure adapted from reference 17.

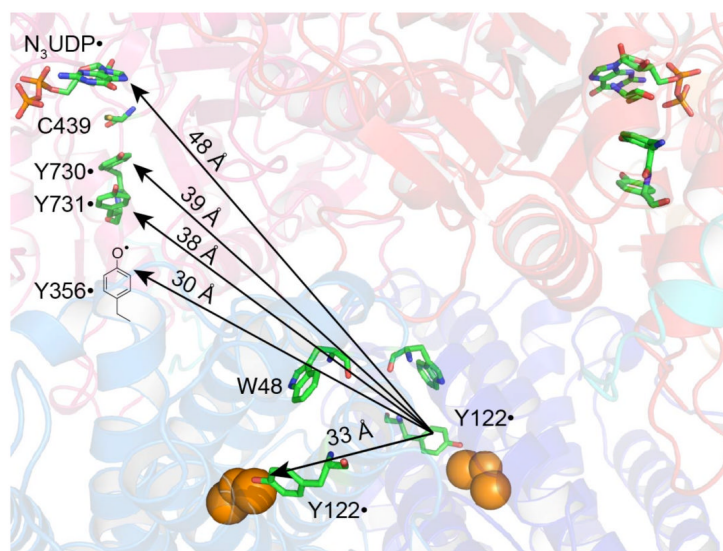


Figure 8. Validating the docking model by PELDOR spectroscopy. By exploiting the half-sites reactivity of RNR, diagonal distances between Y_{122}^{\bullet} on one / pair and $DOPA_{356}^{\bullet}$, $NH_2Y_{731}^{\bullet}$, $NH_2Y_{730}^{\bullet}$, and an active-site N^{\bullet} on the second / pair have been measured.^{20,23} The pathway residues and S were built in from the docking model,² in which Y_{356} is invisible.

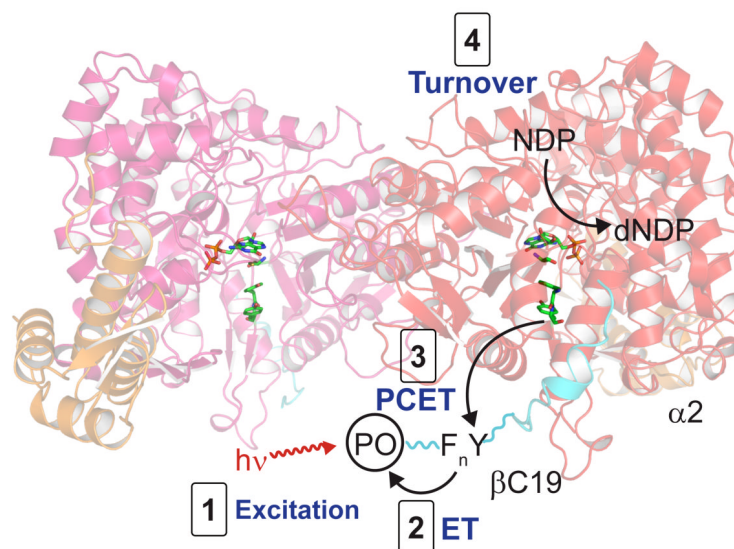


Figure 9. Photo-initiated radical propagation in PO-Y- C19 photopeptides. A photooxidant (PO, black circle) is appended to the N-terminus of a peptide corresponding to residues 356-375 of 2 (C19, cyan), with either Y or F_nY at position 356. Light excitation (step 1) induces oxidation of the residue at position 356 (2), a fraction of which is reduced by Y₇₃₁ of 2 (3). The photopeptide/wt- 2 complex is capable of generating dNDP (4), providing direct evidence for radical injection from the peptide. Figure constructed from PDB ID 1RLR.²

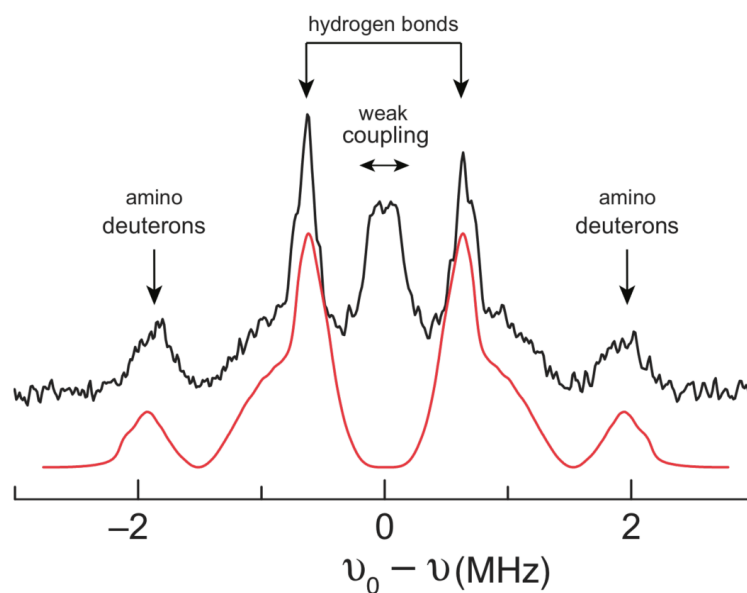


Figure 10.

The 94 GHz [2H]-MIMS ENDOR spectrum of $\text{NH}_2\text{Y}_{730}\bullet$ in the active 2 2 complex reveals the details of its intra- and intermolecular H-bonds. Experimental data are shown in black and a simulation in red. The two prominent peaks centered around 0.6 MHz fall in a region expected for coupled H bonds. The detailed analysis of the experimental spectrum and its simulation is described in reference 21.

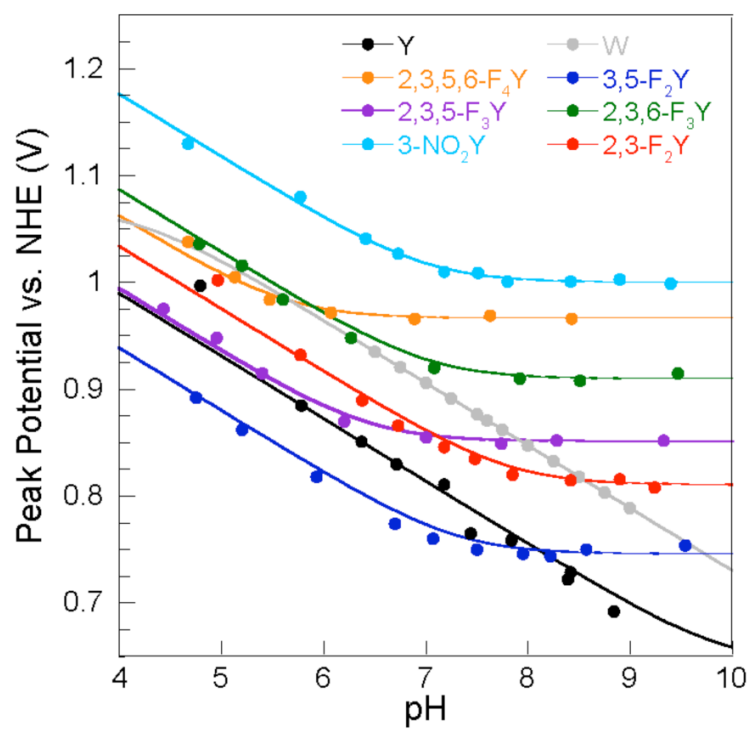


Figure 11. Solution peak potentials ($E_{p,s}$) of Y, W, and UAAs blocked with N-acetyl and C-amide functionalities.^{15,18}

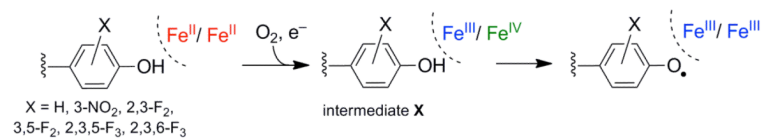


Figure 12. Assembly of the diferric- $\text{Y}_{122}\bullet$ (or $\text{NO}_2\text{Y}_{122}\bullet$ or $\text{F}_n\text{Y}_{122}\bullet$) cofactor from diferrous-2, O_2 and reductant.

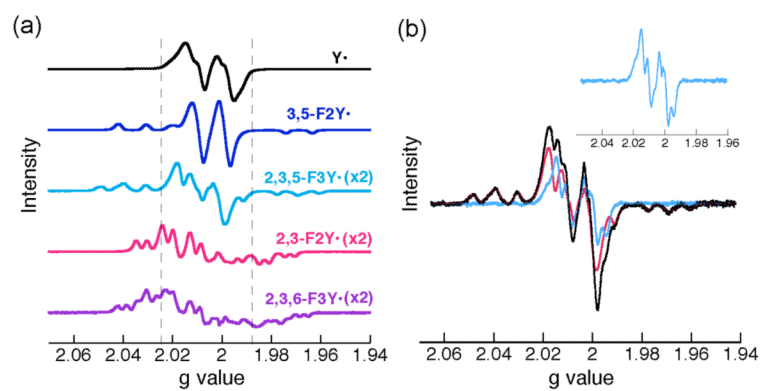
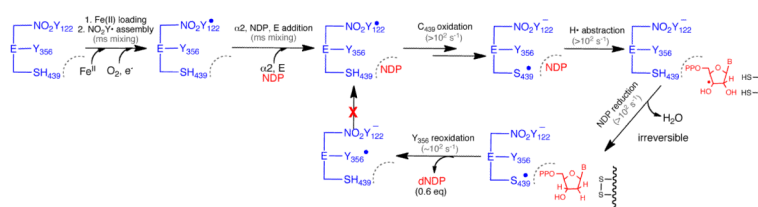


Figure 13.

(a) X-band EPR spectra (77 K) for *E. coli* $Y_{122}\bullet$ and $F_nY_{122}\bullet$ s normalized for radical concentration. Dashed lines highlight the increased spectral width of the $F_nY_{122}\bullet$ s.^{13,14} (b) EPR spectrum of the reaction of $Y_{122}(2,3,5)F_3Y-2$, wt-2, CDP, and ATP quenched at 25 s. The reaction spectrum (black) is a composite of two species: $2,3,5-F_3Y_{122}\bullet$ (pink) and a new radical (blue, magnified in inset), assigned as $Y_{356}\bullet$.¹³

**Scheme 1.**

Kinetic model for radical initiation in the reaction of $Y_{122}NO_2Y-2$ with wt-2, S, and E.²⁹

Table 1

p*K*_as and E_ps of UAAs

UAA ^a	p <i>K</i> _a ^b	E _p vs NHE (V) ^c	E _p vs Y/Y• (mV) ^c
Y	9.9	0.83	-
DOPA	9.7	0.57	-260
NH ₂ Y	~10	0.64	-190
3,5-F ₂ Y	7.2	0.77	-60
2,3-F ₂ Y	7.8	0.86	+30
2,3,5-F ₃ Y	6.4	0.86	+30
2,3,6-F ₃ Y	7.0	0.93	+100
2,3,5,6-F ₄ Y	5.6	0.97	+140
NO ₂ Y	7.2	1.02	+190

^aFor Y, NO₂Y, and F_{*n*}Ys, measurements made on N-acetyltyrosinamide forms.

^bThe solution p*K*_as reported here are perturbed by <+1 unit at positions 356, 730, and 731 and by >+2.5 units at position 122.

^cAt pH 7, as reported in references 15,17-19 and references therein.